AD NUMBER

AD845761

NEW LIMITATION CHANGE

TO

Approved for public release, distribution unlimited

FROM

Distribution authorized to U.S. Gov't. agencies and their contractors; Administrative/Operational Use; SEP 1968. Other requests shall be referred to Rome Air Development Center, Griffiss AFB, NY.

AUTHORITY

RADC ltr, 14 Oct 1971

RADC-TR-68-465
Final Report, September 1968

INTERFEROMETRIC MEASUREMENTS ON SECEDE I BARIUM RELEASES

Robert W. Deuel
Robert D. Sears

Contractor: IIT Research Institute
Contract Number: F30602-68-C-0344
Effective Date Of Contract: 19 April 1968
Contract Expiration Date: 15 September 1968
Amount of Contract: $15,242
Program Code Number: 8E20

Principal Investigator: Robert D. Sears

Project Engineer: Raymond Urtz, Jr.
Phone: 315 330-3443

Sponsored by
Advanced Research Projects Agency
ARPA Order No. 1057, Amend No. 2

Rome Air Development Center
Air Force Systems Command
Griffiss Air Force Base, New York

INTERFEROMETRIC MEASUREMENTS ON SECEDE I BARIUM RELEASES

Robert W. Deuel
Robert D. Sears

IIT Research Institute

This research was supported by the Advanced Research Projects Agency of the Department of Defense and was monitored by Raymond Urtz, Jr. RADC (EMASA), GAFB, N.Y. 13440 under Contract No. F30602-68-C-0344.

REPORT SUMMARY

The purpose of this research project was to evaluate an optical technique for the determination of ion densities in a high altitude chemical release of barium. The method involved the detection of the isotopically shifted hyperfine lines of barium ions whose emission was less likely to be optically thick due to their minor abundance and lower relative transition probability. Thus, emission intensities could be readily related to the ion population. Simultaneous detection of a neutral and an ion emission line could also be accomplished with this instrument to provide data regarding the ionization conversion process at early times.

The basic instrument is a Fabry-Perot interferometer which is magnetostrictively scanned offering high wavelength resolution and high background rejection. The instrument and its associated equipment were government furnished through the Defense Atomic Support Agency. Added equipment consisted of narrow band optical filters for the barium lines of interest.

Data were obtained for the releases Apple and Dogwood but sufficient data from which a time history could be developed were obtained only on the latter event.

Hyperfine emission features were observed for the barium ion line at 4934 A from which upper excitation level populations

were dervied. Calculations were made to determine the ratio between total ion population and that of the upper energy level giving rise to the 4934 A line. Measured intensities are then presented as barium ion column densities and as volume densities by consideration of the pnotographically derived cloud dimensions; the latter results agree with the radar measurements of electron density. A measure of the neutral/ion ratio was also determined for two points at early times. The results thus indicate that the proposed technique is useful in the determination of ion density in the cloud with spatial resolution of 0.3 degrees.

INTERFEROMETRIC MEASUREMENTS ON SECEDE I BARIUM RELEASES

Robert W. Deuel and Robert D. Sears
IIT Research Institute
Chicago, Illinois 60616

I. OBJECTIVES OF THE EXPERIMENT

A high resolution, magnetostrictively scanned Fabry Perot Interferometer was fielded on the SECEDE I experiment by IIT Research Institute personnel. The overall objective of the IITRI experiment was to evaluate an optical measurement technique by which Barium ion densities in the cloud may be determined. The high spectral resolution (0.02A) of the instrument allows detection of isotope shifted hyperfine lines of BaI and BaII. Because of the lower density of the minor barium isotopes (135 and 137) and the consequent longer optical path in the cloud for the hyperfine lines, these spectral components may provide an "optically thin" measure of Ba neutral or ion density when the main isotope (138) lines are "optically thick". In addition, the scanning capability of the instrument allows simultaneous intensity measurement of two closely spaced lines 6498.78 and 6496.9A which are scattered by BaI and BaII respectively. Thus the BaI to BaII conversion process may be followed in early times. Finally, the high spectral resolution of the instrument allows detection of the resonance lines even against a high background of scattered sunlight. It was the goal of this part of the experiment to follow the Barium ion cloud into full daylight.

II. DESCRIPTION OF THE EXPERIMENT

A. Equipment

The interferometer optical unit consists of a single magnetostrictively scanned Fabry-Perot etalon preceded by a narrow band dielectric filter (on the order of 0.1% of the wavelength). The spacing of the interferometer plates is about 5 mm defining a free spectral range of 0.24 Å at 4934 Å and 0.43 Å at 6498 Å. The light admitted by the force filter thus contributes about 20 orders at the lower wavelength and 10 at the higher wavelength. Selection of the filters and features observed prevented unwanted contamination from other lines in other orders. The disadvantage of this mismatch occurs at late times after the release when the increasing scattered sunlight is admitted in these multiple orders thereby decreasing the optimum signal to noise ratio.

The optical geometry of the interferometer unit defines a field of view of about a third of a degree with a one inch collector aperture. Pointing of the input axis is accomplished by a two-axes rotating prism mount in front of the collector aperture. Sighting is performed through a parallel prism and telescope arrangement. The fore filter for the instrument is mounted in a sliding tray which has provision for two separate filters allowing sequential observations of two features.

The scanning interferometer system was designed to integrate successive wavelength scans in a coherent manner by incorporating a mercury trigger line on an off axis path. The

light enters through a fiber optic pipe at the field-defining input aperture and is detected through another fiber optic pipe at the corresponding point at the output aperture. Detection of the trigger signal thus provides an accurate wavelength calibration for subsequent data in each scan of the etalon. In order to prevent contamination of the main detector output from scattered mercury light, the trigger light source is blocked by a shutter after the line is detected.

The main photomultiplier output observes the central fringe at the output aperture which corresponds to different wavelengths as the interferometer plates are magnetostrictively scanned. To enhance detection of weak signals against a strong background, the output signal is digitally recorded in a multi-channel analyzer where each pulse represents a photon interaction in the PM. The time dependent sweep of the analyzer and the current through the interferometer bars produces a direct correlation between channel number and wavelength. The mercury trigger signal is then used to start the analyzer sweep at the same wavelength point for coherent addition of successive scans. This real time integration and display of the channel count permitted integration until the desired spectral feature was observed with subsequent readout or storage of the data to provide maximum time resolution. This technique was used during the field tests to simultaneously monitor total system operation and to select the optimum data accumulation/readout cycle.

The system was generally operational prior to this field

experiment and it was only necessary during the first phase of the work to set up the system in the laboratory for check out. New coatings were required for the interferometer plates to provide the required spectral resolution throughout the range of interest; the resolution of the instrument is directly related to the reflectivity of the coating at the desired wavelength. By this stage of the preparations, it was decided that the primary features to be observed were the ion lines at 4934 Å and 6496 Å and the neutral line at 6498 Å; the latter two lines would be observed simultaneously in different orders through the same fore filter. It was thus necessary to specify high (90%) reflectivity from about 5000 Å to 6500 Å for the plates of the etalon. The requisite narrow band fore filters were also ordered at this time.

Successful check out of the system was completed prior to shipment of the equipment to Ramey Air Force Base, Puerto Rico. The site chosen to provide maximum observational capability was the Foreign Broadcast Information Service facility near Corozo in southwestern Puerto Rico near one of the phototriangulation sites. The equipment arrived, was set up and completely operational during the week before the planned first shot of May 2.

B. FIELD OPERATION

The following log summarizes activity during the test series.

May 2	Thur.	Operational 02:30; attempted calibration aborted due to condensation on interior optical components; 4934 Å and 6498 Å filters installed. Launch 0512. One data record obtained for 4934 Å, integrated from T+20 to T+240 seconds.
May 4	Sat.	Operational 02:45; mission scrubbed at T-10 minutes. System checks with sodium lamp.
May 5	Sun.	Operational 02:45; mission scrubbed 03:45.
May 7	Tues.	Operational 02:30; launch 05:00 (-12.5°). Operate until 05:55. Analysis indicates no data obtained this shot.
May 8	Wed.	Operational 03:00; mission scrubbed 03:45; azimuth and elevation corrections for Corozo noted with respect to Parguera.
May 12	Sun.	Operational 03:30; launch 05:06; second stage observed, no release, and no data.

May 13	Mon.	Operational 03:20; launch 05:08; operate until 05:14; 8 data records for 4934 A to T+24 minutes and for 6498 Å, three records from T+0 to T+150 seconds. Calibration for resolution performed after completion of test data.

III. DESCRIPTION OF THE DATA

A. Acquisition

The release clouds were successfully acquired on the telescopic viewfinder of the interferometer on Haven Barter I and IV. On Haven Barter II, the release cloud faded from view before the interferometer field of view could be adjusted properly in azimuth and elevation. No release took place on Haven Barter III.

During the first event, a 35 mm camera was attached to the tracking telescope to provide specific data regarding pointing direction for correlation to the line emission measurements. Visual sighting for manual tracking was then accomplished through the reflex optics of the camera. It was immediately apparent during the first event that the extent of the barium cloud and the relatively low contrast obtained at the camera view finder made tracking extremely difficult. Thus, the paucity of data during the first event is at least partly ascribed to poor tracking of the cloud. The camera was removed from the sighting telescope for the subsequent events where the pointing direction was indicated on sketches of the cloud structure. Tracking problems remained, however, because the telescope's field of view was smaller than the cloud size except at very early times and also because of the inability to visually locate the cloud at late times. These problems very likely contributed to the variance of data during the observation as well as the termination of data when the back-

ground increased.

Observations were made during the second event but analysis of the data revealed no evidence of line emissions. Although operational for the third event, the apparent malfunction of the payload precluded data acquisition.

The fourth event produced eight sets of intensity measurements for the 4934 Å ion line from T+3 minutes to T+23 minutes and two sets of intensity measurements for the 6498 Å neutral and 6496 Å barium ion line from T+30 seconds to T+180 seconds.

B. Hyperfine Structure and Line Shape

The interferometer scanning interval was set to cover slightly more than two orders for both the 4934 A line and the 6496.9 and 6498.78 A lines. Hence, placement of the lines with respect to the free spectral range resulted in reproduction of three main peaks for the 4934 A line, and two sets of peaks of the 6496.9 and 6498.78 A lines. The spectral intensity which is expressed as a count rate versus wavelength in terms of the counting channel assignment is illustrated in Figure 1. Because the wavelength scan is somewhat non-linear in relation to the driving current and hence non-linear in channel assignment (time), the third order peak at the right side of the 4934 A display is wider than the first and second orders. The same effect may be noted on the 6496.8 A plot.

Instrumental characteristics determine the ability to

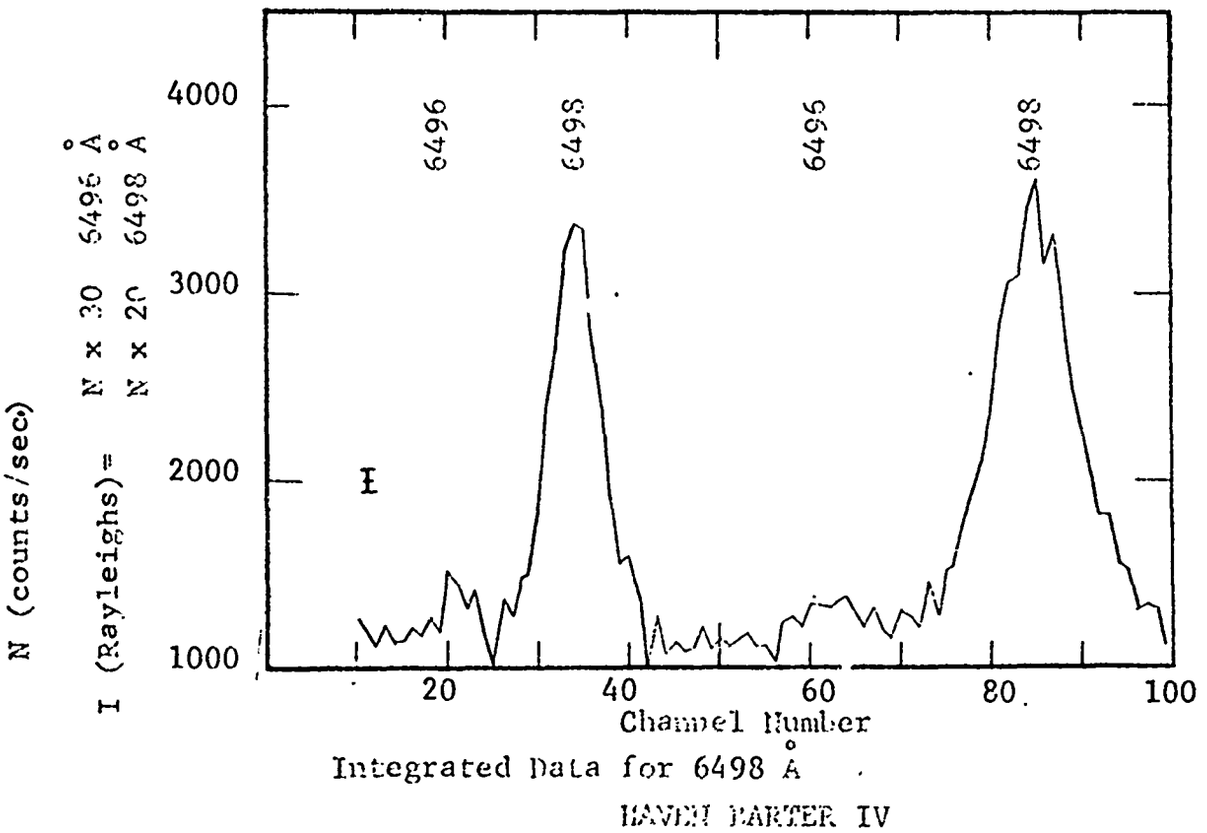

Integrated Data for 6498 Å

HAVEN PARTER IV

(a)

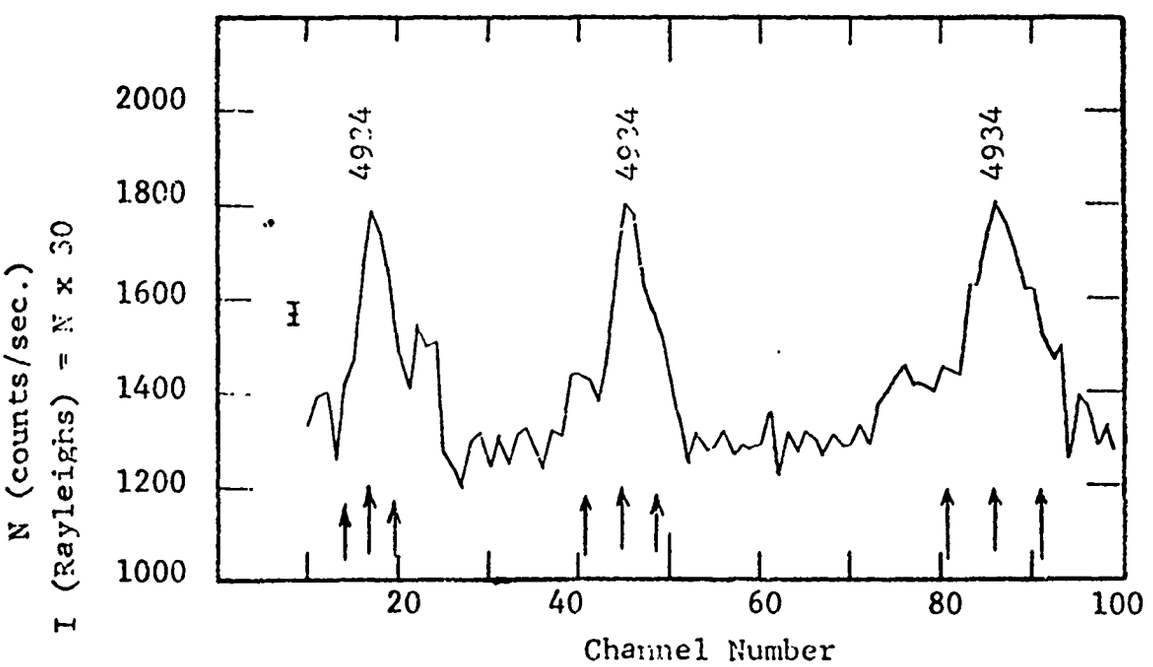

Integrated Data for 4934 Å

HAVEN PARTER IV

(b)

FIGURE 1

resolve the hyperfine structure on the 4934 A line. The hyperfine lines are located at separations of $\pm$ 0.026A, $\pm$ 0.034 A, and $\pm$ 0.038A from the main emission peak. The instrumental resolution for the 4934 A and for the 6498 A region is determined by the free spectral range and by the finesse of the etalon plates. These quantities are listed in the following table together with the observed line characteristics.

TABLE 1

WAVELENGTH	FREE SPECTRAL RANGE	FINESSE	RESOLUTION	OBSERVED LINE WIDTH
4934 A	0.24 A	17	0.014 A	0.04 A
6498.78 A	0.43 A	13	0.033 A	0.05 A

The observed line widths for the main emission peaks were much larger than expected insofar as the doppler width of 0.008A (corresponding to an ionospheric temperature of 800°K) would place the natural line within one or two time-spectral resolution channels. The instrumental characteristics were carefully examined in order to ascertain positively that the line width was not primarily an internal effect. Lack of any clear-cut instrumentation line broadening effects leads to the conclusion that the observed line breadth is real and that it is an effect of the optical depth of the emitting medium. Comparison of the line widths with an idealized Gaussian profile for a 800°K doppler broadened line indicates that the true peak emission intensity is a factor of at least 2 to 3 higher than the observed

peak. As will be seen, this conclusion conforms with that made by comparison of the main line observed intensity values with the intensity of the hyperfine structure lines.

The instrumental resolution is adequate to observe the 0.026 A and the 0.034/0.038 A lines. As seen in Figure 1, these lines are of much lower intensity than the main line, however, they appear consistently in all of the 4934 A data in the same wavelength channels. It is possible to determine the intensity of the hyperfine emissions by subtraction of the main line profile and background count rates from the peak count rate in the hyperfine line channels. Because the hyperfine lines are expected to be optically thin, and they lie in at most two wavelength channels, the single channel peak value is a reasonable estimate of the total hyperfine line intensity.

The results for the fourth event (6804 Dogwood), shown on Figure 2, indicate a roughly constant level for the 4934 Å primary peak (Ba 138) throughout the observation period from T+3 to T+23 minutes. It is noted that the largest deviation from the constant level at T+5.5 minutes corresponds to an observation near the edge of the cloud while all other measurements correspond to positions near the center of the ion cloud. For comparison, the isotope line intensity is shown normalized to account for the difference in relative abundance of the respective species (135/137 to 138) and for the difference in transition probability. The intensity of the barium ion isotope line appears to decrease during the first twelve minutes with the subsequent two data points at T+20 and T+22 minutes indicating an increase. Although the error limits are on the order of a

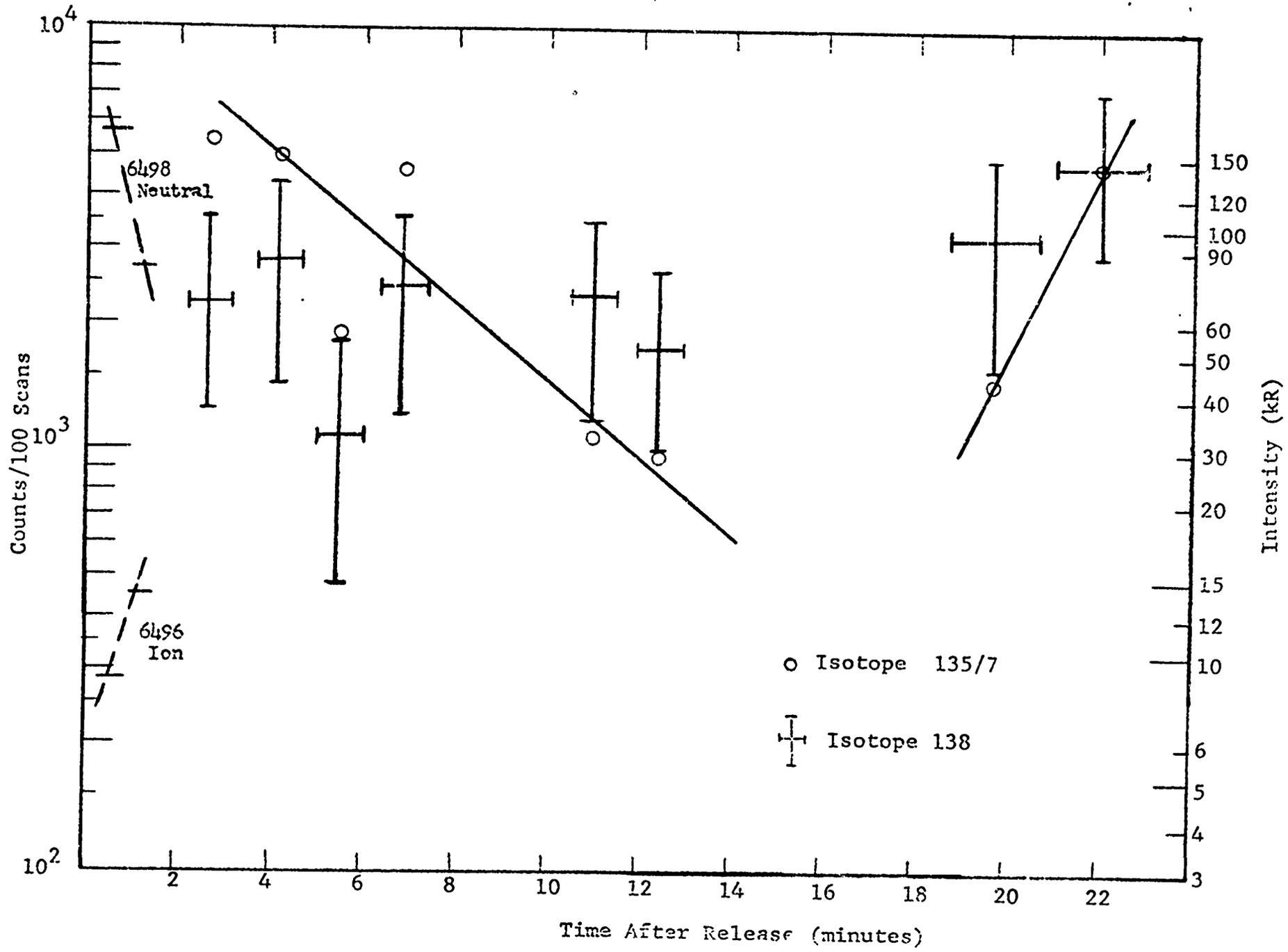

Figure 2 Time History of 4934 A BaII, Haven Barter IV

factor of two or three, this interpretation of the time history is consistent with the data of the primary 138 isotope which indicates optical thickness at times less than T+10 minutes.

C. Neutral/Ion Intensity Ratio

Figure 1 shows average data for both the 6498/6 A and 4934 A lines; the upper curve is the integration of the three sets of data totaling 100 scans (at one second/scan) for the 6498/6 A neutral and ion lines; the lower curve is the integrated data for five of the eight sets of measurements for the 4934 A ion line totaling 300 scans. The primary feature observed in the first case is the neutral barium emission at 6498.76 A seen in two successive orders. At approximately ten and twenty channels to the left of this feature for the first and second orders respectively, there is observed a minor increase in intensity in the appropriate channel for the ion line at 6496.90 A. Assuming this identification, the average background is subtracted from these channels to provide ion intensity data corresponding to the readily determined neutral line intensity. In Figure 2, two points are plotted for each of these lines showing the decay of the neutral and the growth of the ion emission. A third point for each line at T+2 minutes is in the noise level negating comparison. However, the first two points may be used to obtain decay and growth rates for the neutral and ion emission respectively. An exponential fit to these points provides a 1/e decay time for the 6498 A neutral barium line of about 24 seconds and an e-folding increase for the 6496 A barium ion line of about 60 $\pm$ 30 seconds. It is noted here that the figure shows count

rates per second which are related to intensity by the transmission of the fore filter at the wavelengths of the spectral lines. The varying transmission results in an intensity ratio of two-thirds the count rate ratio. Thus,

TABLE 2

Time	6498 6496 Intensity (Neutral/Ion) Ratio
T+42 sec.	12
T+72 sec.	4

When the signal at 6498 A was lost in the noise level at T+2 minutes, the interferometer was switched to the 4934 Å filter. Subsequent observations were made at 6498 A but no further data were obtained.

IV. DETERMINATION OF ION POPULATION

The direct data obtained in this experiment in counts per second per unit wavelength correspond to the input intensity in photons per second within the same wavelength interval. The photon counting technique is better than 90% efficient for the count rates encountered here. Considering overall optical efficiency of the instrument, the quantum efficiency of the photomultiplier, the field of view, and the collector aperture, the following relation is obtained.

$$I_{source} \left(\frac{photons}{sec\ cm^2}\right) = 1.82 \times 10^8 \times N \left(\frac{counts}{sec}\right) \quad (1)$$

It is noted here that the derivation of this relation involved the correlation of the count rate at late times (T+30 to 40 minutes when the signal is due to scattered sunlight) with published data for scattered sunlight versus solar angle. The empirical proportionality constant thus contains a lumped parameter including lens and filter transmissions, mirror and prism reflectivities, interferometer transmission, and PM quantum efficiency. This pseudo-calibration procedure likely provides the most realistic conversion due to the inherent inclusion of the total system function but it is recognized that greater precision with proper calibration is highly desirable. This point should be remembered in the interpretation of the derived data.

A. Intensity versus Number Density (Excited State)

A linear relation between observed intensity and the number density of the upper level giving rise to the observed

radiation holds for the region where the line is said to be optically thin. The addition of more emitters along the line-of-sight path does not then produce a corresponding increase in intensity due to the occurrence of self-absorption. The relation between observed intensity and line density (volume density x path length) can be calculated for a pure Doppler broadened line (Plass 1958) and the result is shown in Figure 3 for the BaII 4934 Å line. The linear relation holds for (NL) less than 10^{11} while beyond 10^{13} the intensity is proportional to $(\ln NL)^{1/2}$; the latter region is where the line is said to be optically thick.

Observation of the hyperfine lines of the BaII 4934 A line should provide a source whose intensity is about a factor of 20 less than the primary line andwhich is thus more likely to be optically thin. From the electron density data at times corresponding to the optical data, the ion number density is between 10^6 and 10^7 with an ion cloud radius between 2 and 3 km (Rosenberg); the resulting ion line density is 5×10^{11} to 5×10^{12}. Considering the factor of twenty reduction in relative emission for the isotope line, its intensity should fall in the region shown on the lower curve in the figure. The derived values for ion line density may later be examined on this figure to determine if corrections are necessary for optical thickness.

The proportion of excited state ions for the BaII 4934 isotope transition to the total barium ions in this state is 1/21.9. The line density is then found from the isotope emission intensity as follows:

$$N_4 L = 21.9 \frac{1}{A_{41}} \times I_{135/7} \quad \frac{\text{photons}}{\text{sec cm}^2} \qquad (2)$$

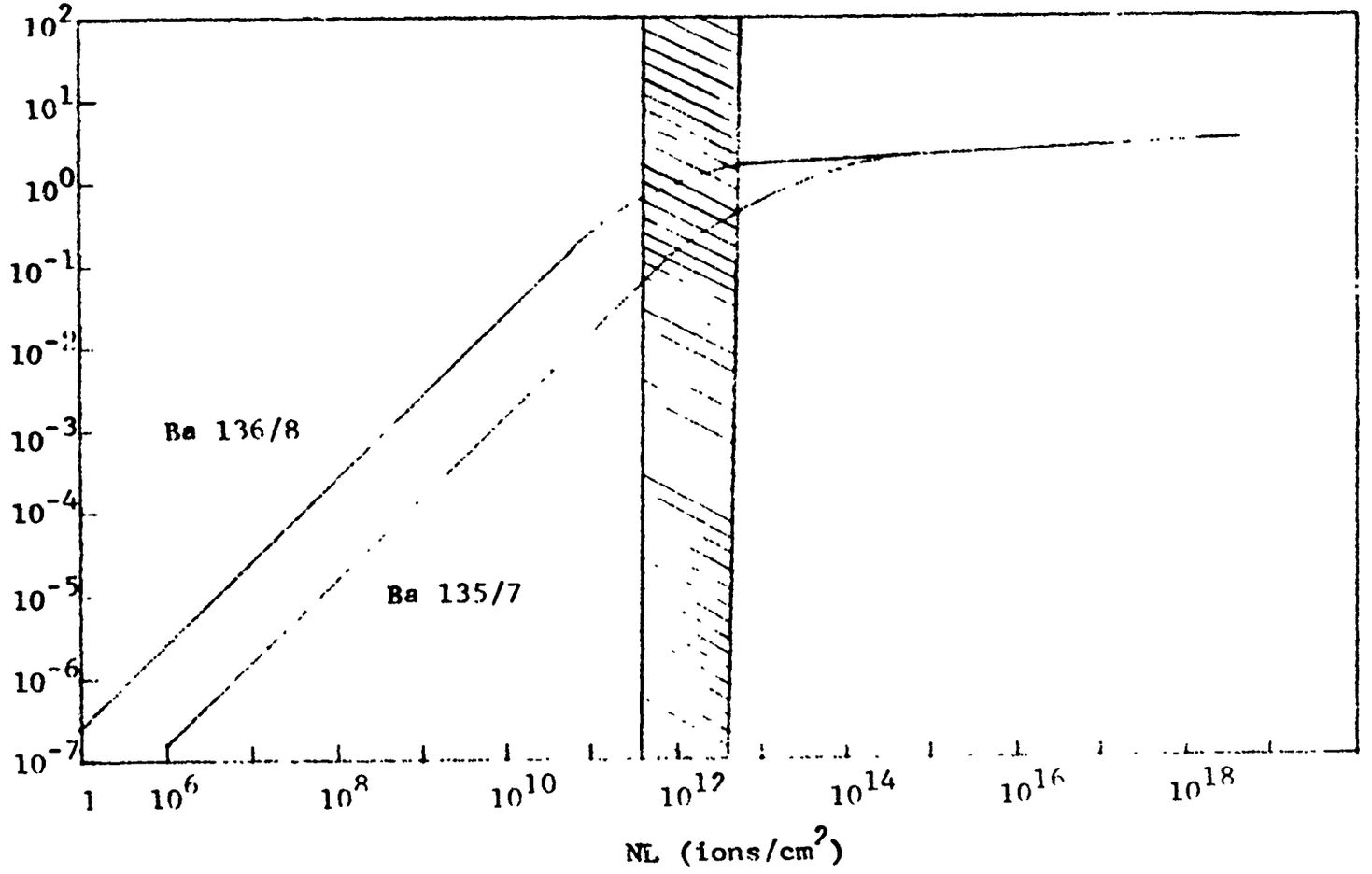

Figure 3

Intensity versus Line Density for Ba II 4934 Å Emission

where N_4 is the number density of barium ions in the $^2P_{1/2}$ level, L is the optical path length, and A_{41} is the Einstein transition probability for 4934 Å emission. In order to determine the total ion population, it is necessary to determine the relative populations of barium ions in all possible states to find the ratio of N_4/N_{Total}. The following section will discuss the excitation processes and provide calculations of the ratio of total ions to ions in the upper level of the 4934 A line.

B. Population of BaII States

Both radiative and collisional excitation processes will be considered to determine the relative excitation rates.

B.1 Collisional Excitation

Considering two Maxwell-Boltzmann distributions, one of BaII (ground state number density = N_1) and one for an electron and proceeding in a manner similar to that indicated in Chapman and Cowling (1960), one obtains the following expression for the rate of collisional excitation of BaII:

$$\frac{dN_{14}}{dt} = \frac{2}{\pi} N_1 N_e \left(\frac{2\,kT}{m^*}\right)^{1/2} \sigma_{ae} \left(1 + \frac{m^* g_o^2}{2\,kT}\right) \exp\left(\frac{-m^* g_o^2}{2\,kT}\right) \qquad (3)$$

where $m^* = \frac{m_1 m_e}{m_1 + m_e}$, g_o is the relative velocity corresponding to the minimum energy below which no excitation occurs,

and σ_{ae} is the atom-electron collision cross section. The derivation of this expression assumes that the same temperature can be applied to each distribution; the case for unequal temperatures is more complex and will not be considered here. With the appropriate cross section (σ_{ae}) and energy $(\frac{m^* g_o}{2})$ equation (3) gives the rate of excitation to a given level. Consider the excitation process:

$$Ba^+ (^2S_{1/2}) + e \rightarrow Ba^+(^2P_{1/2}) \quad E = 20261.5 \ cm^{-1} \tag{4}$$

The barium ion is essentially stationary compared with the electron, so that g_o must be a limiting electron velocity. In the center of mass system used above, the electron can give up only one-half of its energy maximum. Hence $\frac{m^* g_o}{2}$ must equal twice the excitation energy or:

$$\frac{m^* g_o^2}{2 kT} = \frac{2 \times 20261.5 \times 6.6256 \times 3.00 \times 10^{-17}}{1.3805 \times 800 \times 10^{-16}} = 72.9 \tag{5}$$

The electron density, N_e, is $\sim 10^6$ cm^{-3}. Thus equation (3) becomes

$$\frac{dN_{14}}{dt} = N_1 \sigma_{ae} \times \frac{2}{\pi} 10^6 (7.22 \times 10^{14})^{1/2} \times 72.9 \times 10^{-31}$$

$$= N_1 \sigma_{ae} \times 1.2 \times 10^{-16} \ sec.^{-1} \ cm^{-2} \tag{5a}$$

Since σ_{ae} is on the order of 10^{-16} cm^2, equation (5a) reduces to:

$$\frac{dN_{14}}{dt} \sim N_1 \times 10^{-32} \quad sec.^{-1} \tag{5b}$$

B.2 Radiative Excitation

Population of the $^2P_{1/2}$ state from the ground state can also occur by the absorption of radiation according to the relation:

$$\frac{dN_{14}}{dt} = N_1 \; B_{14} \; \rho_{14}(\nu) \tag{6a}$$

where N_1 is the number density in the lower state

Bij is the Einstein transition probability for absorption and $\rho_{14}(\nu)$ is the spectral radiation density at the wavelength of the transition.

The transition probability for absorption (Bij) is proportional to the transition probability for emission (Aij):

$$B_{12} = \frac{c^3}{8 \; h \; \nu^3} A_{21} = 6.55 \times 10^{19} \quad \frac{cm^3}{erg \; sec^2}$$

The excitation source of radiant energy is sunlight which has a spectral density at ~5000 Å of:

$$\rho_\nu(\nu) = \frac{0.20 \times 10^{-4} \times 10^7}{\nu} \times 10^8 \; \frac{ergs}{cm^3} \; sec$$

$$= 5.4 \times 10^{-20} \text{ ergs. sec. cm}^{-3}$$

The radiative excitation rate is then:

$$\frac{dN_{14}}{dt} = N_1 \times 6.55 \times 10^{19} \times 5.4 \times 10^{-20} \text{ sec}^{-1}$$

$$= N_1 \times 3.55 \text{ sec}^{-1} \qquad (6b)$$

These rather detailed calculations for two kinds of excitation processes provide the basis for the following discussion of the order of magnetude for all possible kinds of excitation and de-excitation processes, which may affect the relative populations of the states for the barium ion.

B.3 Other Excitation/De-excitation Processes

All of the events that can populate or depopulate excited states must now be considered if we are to relate an excited state ion concentration to the total ion concentration. We will let N_j be the concentration of ions in the jth excited state (in our case the upper state of the 4934 Å transition). N_1 is the ground state population, N_k the population of the metastable ^2D levels, N_L the combined population of all states above N_j, N_e is the electron density, and α, β, and γ are the various excitation and de-excitation rates. All of the results of this discussion are presented in Table 3.

For the case of collisional excitation, the α was evaluated in the preceding section using a cross-section of $\sim 10^{-16}$ cm^2.

Table 3 shows the value of $10^{-32}\ N_1$ obtained (event type 1). For event type 2, ion and/or atom collision excitation events can be considered approximately equal; the cross section will not be different by more than one or two orders of magnitude from that for atom-electron. Therefore, it is reasonable to assume that event (1) $\sim$ event (2). Events (3) and (4) refer to collisional excitation from the ^2D states; calculations indicate that even if $N_k > N_1$, an upper limit to this inequality would be $\sim 10^8$. Calculations for (5) and (6), based on reasonable values for solar irradiance and the Einstein B coefficients provide estimates of unity times the lower state number density. It is easily seen then that radiative excitation completely dominates and collisional processes can be neglected in the excitation scheme.

The remaining event types refer to the possible loss modes of ions from the $^2P_{1/2}$ level. Event (7) represents the loss from state j due to electron collisional excitation to higher states N_L. Since it is unlikely that the j state population could ever become as large as the ground state population, it is apparent that (7) $<$ (2). Event (8) is less than event (7) because of the lower relative value of the cross section for these respective events. Event (9) may be about 10^2 larger than event (2), because of the possibility of resonance radiation quenching, but certainly no more than this. The direct radiation loss (10) depends simply upon the radiative lifetime, here assumed to be 10^{-8}. Events (11) and (12) represent the radiation absorption loss and recombination loss; both are of the order N_j. Thus

TABLE 3

ORDER OF MAGNITUDE COMPARISON OF COLLISIONAL AND RADIATIVE EVENTS

CONTROLLING THE POPULATION OF AN EXCITED ENERGY STATE j

Type of Event	No. of Events/ cm^2 -sec	Quantitative Estimates and Comparisons
(1) Electron Collision Excitation from the Ground State	$\alpha_j N_1 N_e$	$10^{-32} N_1$
(2) Heavy Particle Collision Excitation from the Ground State	$\alpha_j N_1 N_i$	$\sim$(1)
(3) Electron Collision Excitation from the k^{th} state	$\alpha_j N_k N_e$	$10^{-24} N_1$
(4) Heavy Particle Collision Excitation from the k^{th} state	$\alpha_j N_k N_i$	$\sim$(3)
(5) Radiative Excitation from Ground State	ρ_{j1}	N_1
(6) Radiative Excitation from k^{th} state	ρ_{jk}	N_k
(7) Electron Collision loss to higher states 1	$\alpha_{jL} N_j N_e$	(7) < (2)
(8) Super elastic electron Collisions	$N_j \beta_j N_e$	(8) < (7)
(9) Deactivitation Collisions with Heavy Particles	$N_j \gamma_j N_i$	(9) $\sim 10^2$ (2)
(10) Direct Radiation Loss	$N_j \frac{1}{\tau_j}$	$10^8 N_j$
(11) Radiation Absorption Loss to Higher States 1	$N_j \beta_{jL} \rho_{jL}$	N_j
(12) Recombination	$\alpha_{je} N_j N_e$	N_j

radiative processes dominate de-excitation as well as excitation processes.

B.4 Reaction Scheme

In order to find the total ion population from the intensity of one ion transition, it is necessary to obtain the relation between the populations of the ^2P, ^2D and the $^2S_{1/2}$ ground state, assuming most of the barium ions are in these states. The excitation rate of the levels higher than ^2P as shown in Figure 4, must be about 1/20th that of the $^2P_{1/2}$ state due to the diminished spectral radiance. Hence these higher levels will be ignored.

The steady state population equations are then:

$$N_4A_{41} + N_5A_{51} = N_1B_{14}\rho_{14} + N_1B_{15}\rho_{15} \tag{7}$$

$$N_4A_{42} + N_5A_{52} = N_2B_{24}\rho_{24} + N_2B_{25}\rho_{25} \tag{8}$$

$$N_5A_{53} = N_3B_{35}\rho_{35} \tag{9}$$

$$N_1B_{14}\rho_{14} + N_2B_{24}\rho_{24} = N_4A_{41} + N_4A_{42} \tag{10}$$

$$N_1B_{15}\rho_{15} + N_2B_{25}\rho_{25} = N_5A_{51} + N_5A_{52} \tag{11}$$

Stimulated emission can be neglected here because the rate relative to that for spantaneous emission is $3.55/10^8$ sec^{-1}. The N's represent the number densities of the respective levels shown in Figure 4 and Aij is the transition probability for emission.

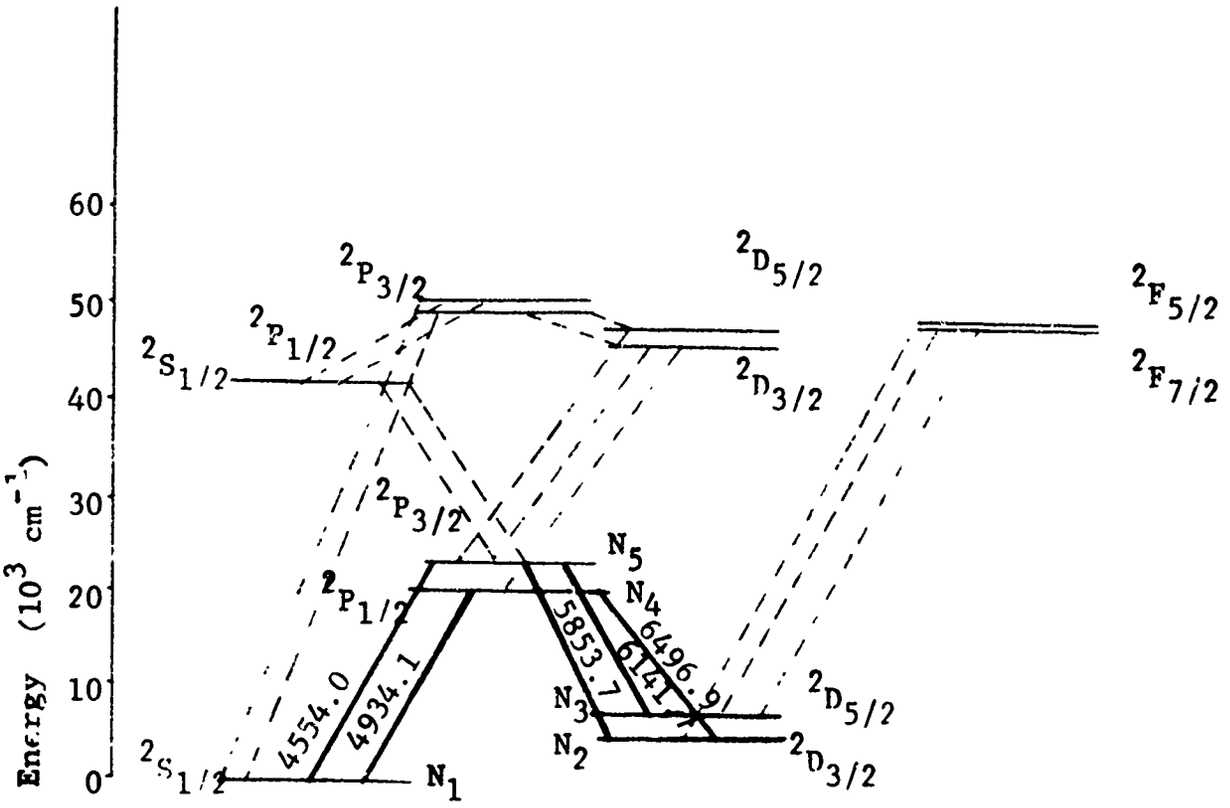

Figure 4 Lower Energy Levels of BaII

——— Transitions of direct interest

N's represent the number densities in each state.

Gallagher (1967) lists the following transition probabilities:

TABLE 4

Wavelength	Designation	Absolute Transition Probability
4554.0	A_{51}	1.18×10^8
5853.7	A_{52}	.048
6141.7	A_{53}	.37
4934.1	A_{41}	.95
6496.9	A_{42}	.33

The B_{ij} values are determined from the A_{ji} following equation (6a) and the $\int_\nu$, (solar spectral radiation density), are obtained from the compilation by H. H. Malitson, NASA, Goddard Space Flight Center. The simultaneous solution for equations (7) through (11) then provides the required population ratios.

$$N_1 = 2.14 \times 10^8 \quad N_4$$

$$N_2 = 0.122 \times 10^8 \quad N_4$$

$$N_3 = 3.11 \times 10^8 \quad N_4$$

$$N_5 = 1.34 \quad N_4$$

$$\text{or } N_{Total} = 5.37 \times 10^8 \quad N_4 \tag{12}$$

NOTE: A calculation was made to determine the relative efficiency of radiative excitation of the $^2P_{1/2}$ level from solar radiation versus optical pumping from radiation in the wings of the Ba 136/138 unshifted line. The result indicates that solar excitation would account for 47% of the total. A correction for this effect is included in the reduction of intensity to ion density.

C. Barium Line Density and Volume Density

Combining equations 1,2, and 12 provides the relation between count rate and ion line density.

$$N \frac{\text{ions}}{\text{cm}^2} = 2.23 \times 10^{10} \times N \frac{\text{cts}}{\text{sec}} \tag{13}$$

Referring again to Figure 3 and recalling that the original data relates to the intensity of the hyperfine isotope line, the effective ion line density below which the radiation may be said to be optically thick is about 2×10^{12} cm^{-2}. All of the data obtained for the BaII 4934 A line lie below this value and thus conform to the linear relation to number density of the emitting specie. The results for the barium ion line density as a function of time for the Test 6804 (Dogwood) are presented in Figure 5. Based upon the preliminary data of Rosenberg, conversion may be made to volume density by using the cloud's optical Gaussian halfwidth. These data are shown in Figure 6 along with the volume electron density measurements by Raytheon. The large scatter of the data points may be ascribed in part to the variability in pointing with respect to the cloud center as discussed in a proceeding section. A linear least squares fit to these points is shown on the figure and indicates a slope similar to that for the electron density change.

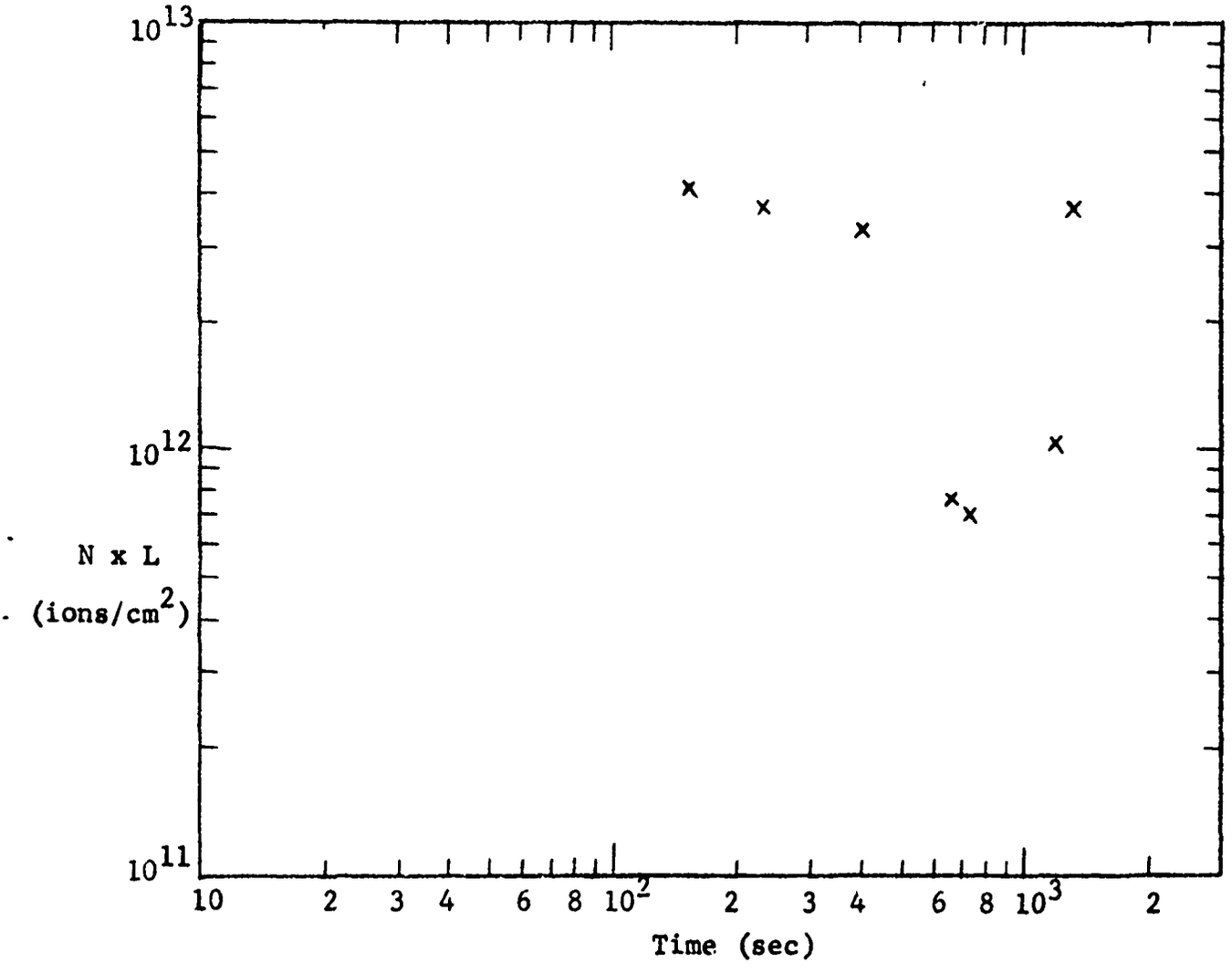

Figure 5. Barium Ion I -e Density

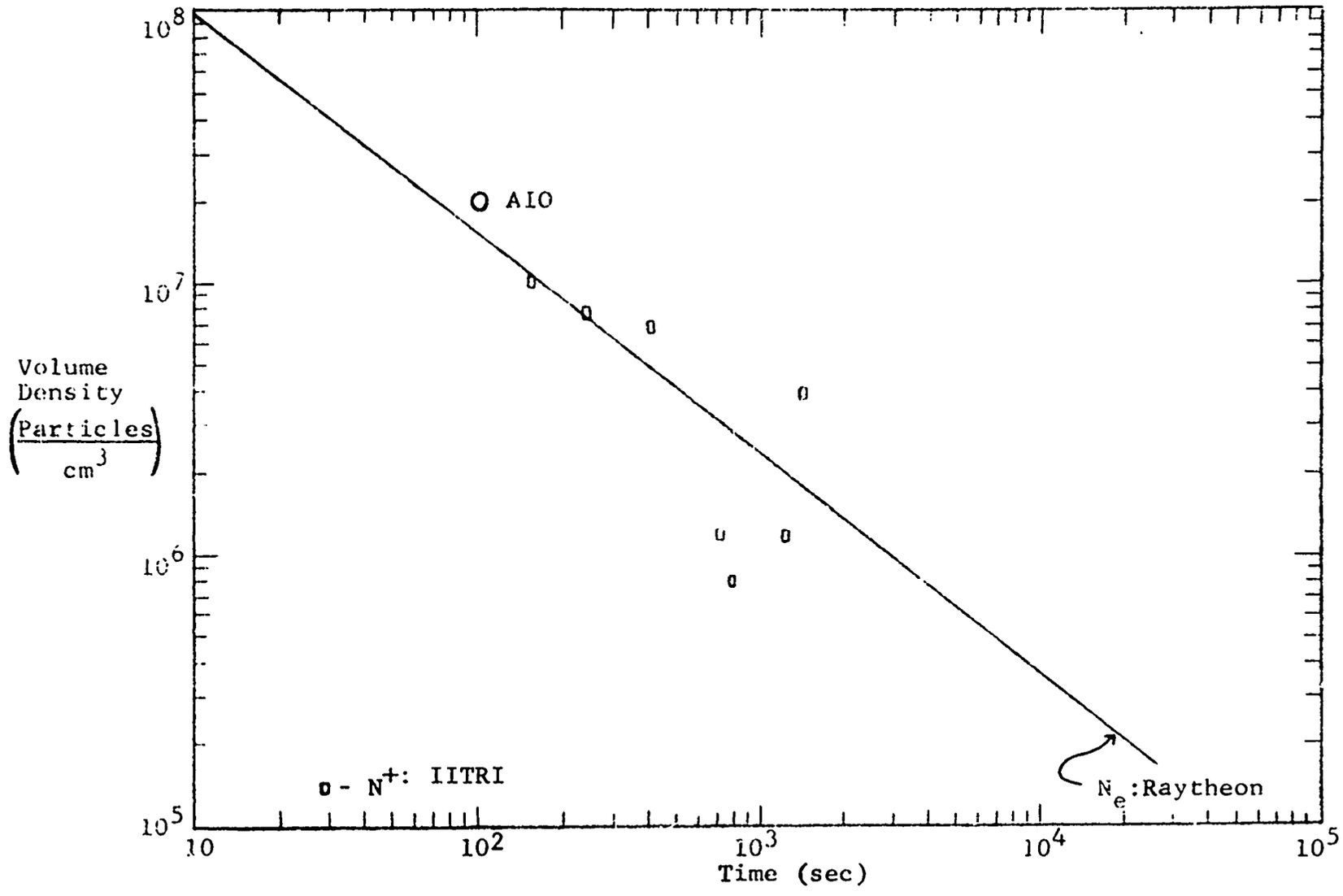

Figure 6. Electron and Ion Time Dependence

V. SUMMARY AND CONCLUSIONS

Measurements of the intensity of resonant scattered emission features from Barium releases in the upper atmosphere have been successfully related to columnar ion density in the Barium cloud. Through adoption of photographic estimates of the Gaussian half width of the released cloud, a peak volume density of Barium ions has been derived. Use of very high resolution interferometric instrumentation has allowed measurement of the isotope shifted hyperfine structure of at least one of the lines (BaII, 4934 A). In addition, by combining line measurements in different orders, simultaneous determination of BaI and BaII density in the early stages of cloud development was shown to be practicable.

General agreement of the temporal behavior of the peak Barium ion volume density values derived herein with the electron density data which were obtained from high frequency radar has been demonstrated. Although absolute value of peak volume density of Barium ions is a factor of about two higher than the peak electron density, this difference is within the error limits imposed by two sources: error in photographic determination of cloud size, and a systematic error source in the calibration which could not be corrected in the field. Based upon these results, it is concluded that the optical measurements of Barium ion density will provide quantitatively accurate and useful results in subsequent experiments.

REFERENCES

Chapman, S., T. G. Cowling, "Mathematical Theory of Non-Uniform Gases", Cambridge University Press, 1960.

Gallagher, A., "Oscillator Strengths of CaII, SrII, and BaII", Phys. Rev. 157, 24 (1967).

Malitson, H. H., "The Solar Energy Spectrum", Sky and Telescope, 29, No. 3, (1965).

Meggers, W. F., C. H. Corliss, B. F. Scribner "Tables of Spectral - Lines Intensities", Part I. Arranged by Elements". NBS Monograph 32, Part I. Dec. 29, 1961.

Plass, G. N. "Models for Spectral Band Absorption", JOSA 48, No. 10, p. 690 (1958).

Rosenberg, N. W., "Barium Releases, Puerto Rico, May 1968".

UNCLASSIFIED

Security Classification

DOCUMENT CONTROL DATA - R&D

(Security classification of title, body of abstract and indexing annotation must be entered when the overall report is classified)

1. ORIGINATING ACTIVITY (Corporate author) IIT Research Institute 10 West 35 Street Chicago, Illinois	2a. REPORT SECURITY CLASSIFICATION Unclassified 2b. GROUP

3. REPORT TITLE

Interferometric Measurements on Secede I Barium Releases

4. DESCRIPTIVE NOTES (Type of report and inclusive dates)

Final Report 19 Apr. 1968 to 15 Sept. 1968

5. AUTHOR(S) (Last name, first name, initial)

Deuel, Robert W.
Sears, Robert D.

6. REPORT DATE	7a. TOTAL NO. OF PAGES	7b. NO. OF REFS
September 1968	36	6

8a. CONTRACT OR GRANT NO.	9a. ORIGINATOR'S REPORT NUMBER(S)
F30602-68-C-0344 b. PROJECT NO. A-8-1662 ARPA Ord 1057-Amend #2 c. d.	V6003-Final Report 9b. OTHER REPORT NO(S) (Any other numbers that may be assigned this report) RADC-TR-68-465

10. AVAILABILITY/LIMITATION NOTICES

This document is subject to special export controls and each transmittal to foreign governments, foreign nationals or representatives thereto may be made only with prior approval of RAD (EMASA), GAFB, N.Y. 13440

11. SUPPLEMENTARY NOTES	12. SPONSORING MILITARY ACTIVITY
Monitored By: Rome Air Development Center (EMASA) Griffiss Air Force Base, New York 13440	Advanced Research Project Agency Washington, D. C. 20301

13. ABSTRACT

The purpose of this research project was to evaluate an optical technique for the determination of ion densities in a high altitude chemical release of barium. The method involved the detection of the isotopically shifted hyperfine lines of barium ions whose emission was less likely to be optically thick due to their minor abundance and lower relative transition probability. Simultaneous detection of a neutral and an ion emission line could also be accomplished with this instrument to provide data regarding the ionization conversion process at early times. Data were obtained for the releases Apple and Dogwood. Hyperfine emission features were observed for the barium ion line at 4934 A from which upper excitation level populations were derived. Calculations were made to determine the ratio between total ion population and that of the upper energy level giving rise to the 4934 A line. Measured intensities are presented as barium ion column densities and as volume densities by consideration of the photographically derived cloud dimensions. A measure of the neutral/ion ratio was also determined for two points at early times.

DD FORM 1 JAN 64 1473

UNCLASSIFIED

Security Classification

04-01: Atmospheric Sciences
Atmospheric Physics

17-08: Navigation, Communications, Detection and Countermeasures - Optical Detection